Highly Tunable Berry Phase and Ambipolar Field Effect in Topological Crystalline Insulator Pb 1− x Sn x Se

ARTICLE *in* NANO LETTERS · FEBRUARY 2015

Impact Factor: 13.59 · DOI: 10.1021/acs.nanolett.5b00172 · Source: PubMed

6 AUTHORS, INCLUDING:

Cheng Zhang
Fudan University
19 PUBLICATIONS **24** CITATIONS
SEE PROFILE

Xiang Yuan
Fudan University
14 PUBLICATIONS **14** CITATIONS
SEE PROFILE

Weiyi Wang
Fudan University
13 PUBLICATIONS **34** CITATIONS
SEE PROFILE

NANO LETTERS

Letter

pubs.acs.org/NanoLett

Highly Tunable Berry Phase and Ambipolar Field Effect in Topological Crystalline Insulator $Pb_{1-x}Sn_xSe$

Cheng Zhang,[†,‡] Yanwen Liu,[†,‡] Xiang Yuan,[†,‡] Weiyi Wang,[†,‡] Sihang Liang,[†,‡] and Faxian Xiu*[,†,‡]

[†]State Key Laboratory of Surface Physics and Department of Physics and [‡]Collaborative Innovation Center of Advanced Microstructures, Fudan University, Shanghai 200433, China

Supporting Information

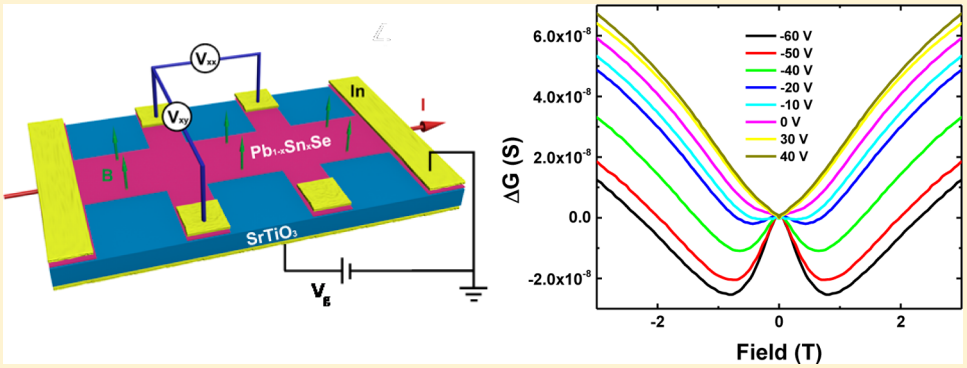

ABSTRACT: Recently, rock-salt IV–VI semiconductors, such as $Pb_{1-x}Sn_xSe$(Te) and SnTe, have been observed to host topological crystalline insulator (TCI) states.[1−7] The nontrivial states have long been believed to exhibit ambipolar field effects and possess massive Dirac Fermions in two-dimension (2D) limit due to the surface hybridization.[8,9] However, these exciting attributes of TCI remain previously inaccessible owing to the complicated control over composition and thickness.[10,11] Here, we systematically investigate doping and thickness-induced topological phase transitions by electrical transport. We demonstrate the first evidence of the ambipolar properties in $Pb_{1-x}Sn_xSe$ thin films. Surface gap opening is observed in 10 nm TCI originated from the strong finite-size effect. Importantly, magnetoconductance hosts a competition between weak antilocalization and weak localization, suggesting a strikingly tunable Berry phase evolution and strong electron−electron interaction. Our findings serve as a new probe to study electron behavior and pave the way for further exploring and manipulating this novel 2D TCI phase.

KEYWORDS: *Topological crystalline insulator, surface state, magnetoconductance, weak antilocalization, ambipolar transport, surface hybridization*

Topological insulators (TIs) are band insulators with a bulk energy gap and helical metallic surface states protected by time-reversal symmetry (TRS).[12,13] The topological surface states originate from its nontrivial band topology and are robust against nonmagnetic disorder, which preserves the TRS.[12,13] Recently, the concept of topological insulators has been extended to a new class of quantum materials, topological crystalline insulators (TCIs).[14,15] Unlike in conventional Z_2 TIs, the topological nature of band structure in TCIs arises from the mirror symmetry instead of the TRS.[14] As a result, the surface states are not confined to the Kramer points and usually consist of even number of Dirac cones.[2,3,15] Moreover, the mirror symmetry can be easily manipulated in comparison with TRS, for instance, via introducing external field or strain, thus making TCI a highly tunable system.[8,15] As proposed in recent studies, when the thickness of TCI is reduced to the two-dimension (2D) limit, the three-dimensional (3D) TCI will transform into a 2D phase with emerged spin-filtered edge states, promising for topological field-effect transistors with high on/off operation speed.[8] Also, a large-Chern-number has been proposed to exist in magnetic doped TCI thin films, making an easy access to the high-temperature quantum anomalous Hall effect.[16] Compared with TI, TCI offers a consolidate platform for exploring symmetry breaking in topological nontrivial systems.[8,15,17]

The rock-salt structure semiconductor SnTe, along with its related compounds $Pb_{1-x}Sn_xTe$ and $Pb_{1-x}Sn_xSe$, has been theoretically predicted to be TCI.[15] Soon after the predictions, angle-resolved photoemission spectroscopy (ARPES) and scanning tunneling microscopy (STM) experiments confirmed the presence of topological surface states in these materials.[1−3] It is well established that PbSe and PbTe, adopting the similar cubic crystal structure, are topological trivial and are expected to be tuned to nontrivial states via lattice strain.[15] Similarly, SnSe is a trivial insulator in the orthorhombic phase but with a relatively large band gap of ∼1 eV.[18] Therefore, in the

Received: January 15, 2015
Revised: February 20, 2015

DOI: 10.1021/acs.nanolett.5b00172
Nano Lett. XXXX, XXX, XXX−XXX

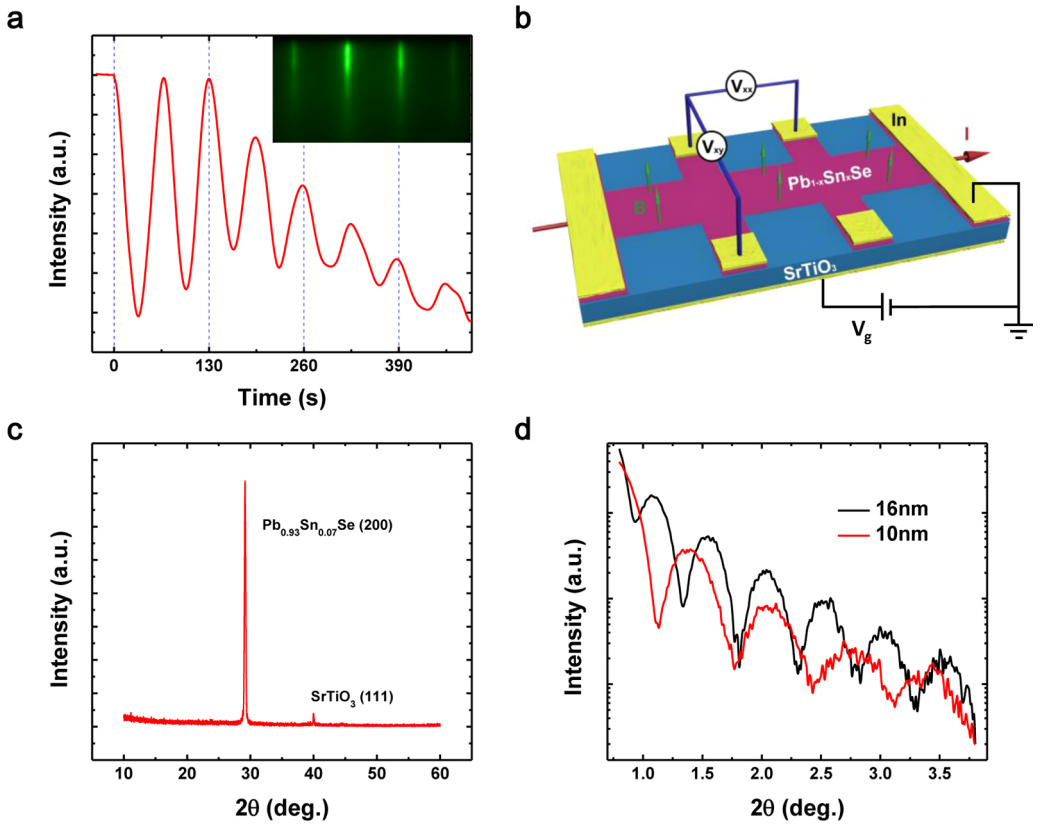

Figure 1. Characterizations and measurement setup of the $Pb_{1-x}Sn_xSe$ thin films and devices. (a) RHEED oscillations, showing the layer-by-layer growth mode. Inset: RHEED pattern of the as-grown film. (b) Schematic device geometry for the magnetotransport measurements of the $Pb_{1-x}Sn_xSe$ thin films. A standard Hall bar geometry is used to measure the magnetoresistance and Hall voltage under various gate voltages and magnetic field. (c) X-ray diffraction pattern of a 16 nm $Pb_{0.93}Sn_{0.07}Se$ thin film. The (200) Bragg peak is clearly seen. (d) X-ray reflectivity measurements of the thin films used to ex situ check the film thickness.

$Pb_{1-x}Sn_xSe$ system two distinct topological phase transitions will occur as the Sn composition x increases.[5] The first one is attributed to the shrink of the lattice constant and the system transforms from trivial to nontrivial states, whereas the second one is a consequence of crystal structure transition, thereby destroying the mirror symmetry and driving the system back to trivial states.[5] Owing to the large gap of SnSe, the $Pb_{1-x}Sn_xSe$ system is believed to be a better platform to study the electric transport behavior of TCI particularly in view of minimizing bulk conduction. In order to explore the intriguing properties of TCI, it is indispensable to realize the ambipolar field effect and achieve the surface dominant conduction, which have not been accessible so far.

In this work, we systematically investigate Sn doping and film thickness-induced topological phase transitions in $Pb_{1-x}Sn_xSe$ (100) thin films grown on $SrTiO_3$ (111) substrates. By varying the Sn concentration from x = 0.07 to 0.43, we observe a crossover from weak localization (WL) to weak antilocalization (WAL) in magnetotransport, showing a transition from topological trivial to nontrivial states. With the film thickness reduced to 10 nm, the top and bottom surfaces hybridize with each other giving rise to the surface gap opening and nontrivial Berry phase collapsing, suggesting a stronger finite-size effect in the TCI system than the previous TI materials.[9,19,20] Importantly, we achieve the ambipolar transport through a gated $SrTiO_3$ substrate with an on−off ratio exceeding 100. The film resistance increases logarithmically as the temperature decreases below 10 K, showing an insulating ground state resulting from a strong electron−electron interaction. Surprisingly, even in the most insulating samples (resistance in 10^8 Ω range), the resistance can be still tuned by magnetic field (more than 7%). It suggests that the electrons possess a long phase coherence length in the material regardless of the short mean free path and strong disorder. Our observation of highly tunable Berry phase points out an interesting interplay between the topological states and the strong electron−electron correlation.

The $Pb_{1-x}Sn_xSe$ thin films are grown on $SrTiO_3$ (111) substrates by molecular beam epitaxy (MBE). Controllable thickness of 10 and 16 nm was achieved with Sn doping concentration varying from x = 0.07, 0.25, 0.32, to 0.43. We specially restrict the Sn concentration to be less than x = 0.45 to avoid the structural phase transition.[5] Figure 1a shows the in situ reflection high energy electron diffraction (RHEED) oscillations during the film growth and the inset is a typical RHEED pattern from 16 nm $Pb_{1-x}Sn_xSe$ thin film. A growth rate of 65s/layer enables a good control of film thickness. A standard six-terminal Hall bar device is used to measure the magnetoresistance and Hall voltage, as schematically shown in Figure 1b. At low temperatures, $SrTiO_3$ exhibits a large relative dielectric constant over 10 000 and can be used as a back gate.[21] The X-ray diffraction (XRD) spectrum can be indexed as (100) plane for 16 nm $Pb_{0.93}Sn_{0.07}Se$ film without detectable impurity phases (Figure 1c). $Pb_{0.93}Sn_{0.07}Se$ was found to adopt cubic phase similar to PbSe. As expected, when we further increase the Sn doping concentration to x = 0.43, there is still no sign of structure phase transition. X-ray reflectivity measurements of

DOI: 10.1021/acs.nanolett.5b00172
Nano Lett. XXXX, XXX, XXX−XXX

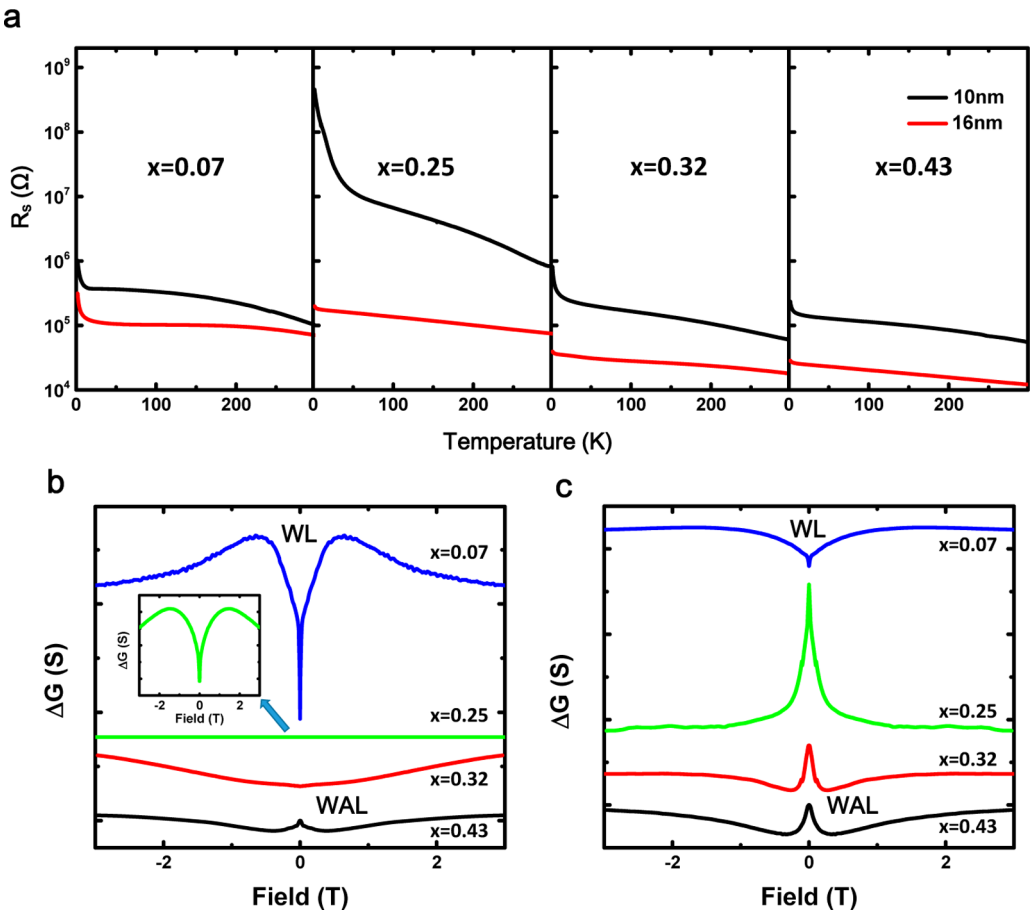

Figure 2. Temperature-dependent resistance and magnetotransport results of the $Pb_{1-x}Sn_xSe$ thin films. (a) Temperature dependence of 2D sheet resistance (R_s) of samples with difference doping composition and thickness. (b,c) Stacked MC $\sigma(B)$-$\sigma(0)$ curves of 10 and 16 nm $Pb_{1-x}Sn_xSe$ thin films with different doping composition x at 2 K, showing a systematic crossover from WL to WAL. (Inset of b) A close-up view of the MC curve with x = 0.25. The MC change in 10 nm $Pb_{0.75}Sn_{0.25}Se$ thin films is several orders of magnitude smaller than the others.

different films were also used to confirm the film thickness, as shown in Figure 1d.

First, the temperature dependence of longitudinal resistance (R_s) was investigated for the obtained $Pb_{1-x}Sn_xSe$ films as displayed in Figure 2a. All the R_s-T curves show a semiconducting behavior at high temperatures (T > 50 K), indicating the Fermi level lying in or near the bulk band gap. As temperature drops below 10 K, R_s increases rapidly in all the samples and such insulating ground state is more pronounced in the 10 nm films. In fact, R_s of the 10 nm films is orders of magnitude higher than that of 16 nm films, and in particular, R_s of 10 nm $Pb_{0.75}Sn_{0.25}Se$ film (x = 0.25) reaches 10^8 Ω range at 2 K (Figure 2a second panel). Even if one considers the enhanced scattering from the underneath substrate in the thinner films, this dramatic increase of resistance is still beyond the normal range. The significant change of resistivity in this scenario suggests that there must be a strong underlying physical mechanism causing the insulating behavior in narrow-gap semiconductors as the system approaches the 2D limit.

In order to clarify the origin, we plot the temperature-dependent R_s in a logarithmic scale, as shown in Supporting Information Figure S2. As represented by the red dash line, R_s is found to be linear with ln(T), a remarkable sign of strong localization.[22] In particular, the samples with x = 0.25 show much higher sheet resistance and exhibit better linear behavior (Supporting Information Figure S2b,f). According to the previous studies,[22,23] the electron−electron interaction needs to be taken into account especially in quasi-2D TI thin films. But in their cases, the highly localized behavior usually becomes pronounced when the thickness is reduced below 3 nm,[22] while in our case the 10 nm films already become very insulating. Therefore, it reveals a strong Coulomb interaction in our $Pb_{1-x}Sn_xSe$ system, consistent with the ARPES results.[5] The unexpected large resistance in 10 nm $Pb_{0.75}Sn_{0.25}Se$ (Figure 2a second panel) reveals a vital role of the electron−electron interaction on the electronic states. Meanwhile, the linear behavior of R_s ~ln(T) survives at higher temperatures as the film becomes thinner, showing a tendency of a stronger localization in the thinner films (Supporting Information Figure S2b). However, this localized behavior contradicts the nonlocal nature of Dirac Fermion in TI.[13,24] To gain an in-depth understanding, we must consider two main factors that contribute to the conductance in TI: the conductance correction from quantum interference(σ^{qi}) and the conductance correction from electron−electron interaction (σ^{ee}). A recent theory proposed that σ^{ee} dominates in the temperature dependence of conductance while σ^{qi} exerts a major influence in magnetoconductance (MC).[24]

Theoretically, spin−orbit coupled surface electrons of TI can generate a nontrivial π-Berry phase in a time reversal closed circuit by scattering trajectories and suppressing backscattering.[12,25] Thus, the destruction of such loops in a magnetic field leads to a negative MC.[26] If a gap is generated on the surface states due to the doping or surface hybridization, the Berry

DOI: 10.1021/acs.nanolett.5b00172
Nano Lett. XXXX, XXX, XXX−XXX

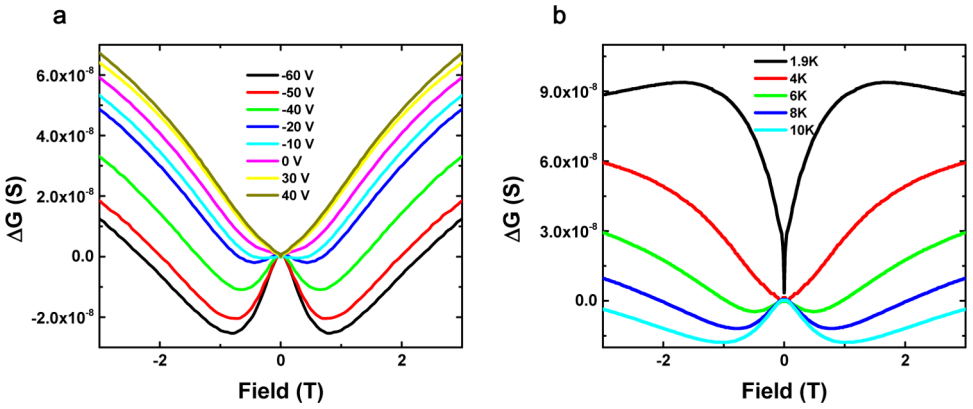

Figure 3. Gate and temperature tunable magnetoconductance of the 16 nm $Pb_{0.93}Sn_{0.07}Se$ thin films. (a) Applying an external gate bias can tune the MC of 16 nm $Pb_{0.93}Sn_{0.07}Se$ thin films from WAL to WL at 2 K as gate voltage changes from −60 to 40 V. (b) Normalized MC $\sigma(B) - \sigma(0)$ of 16 nm $Pb_{0.93}Sn_{0.07}Se$ thin films at different temperature.

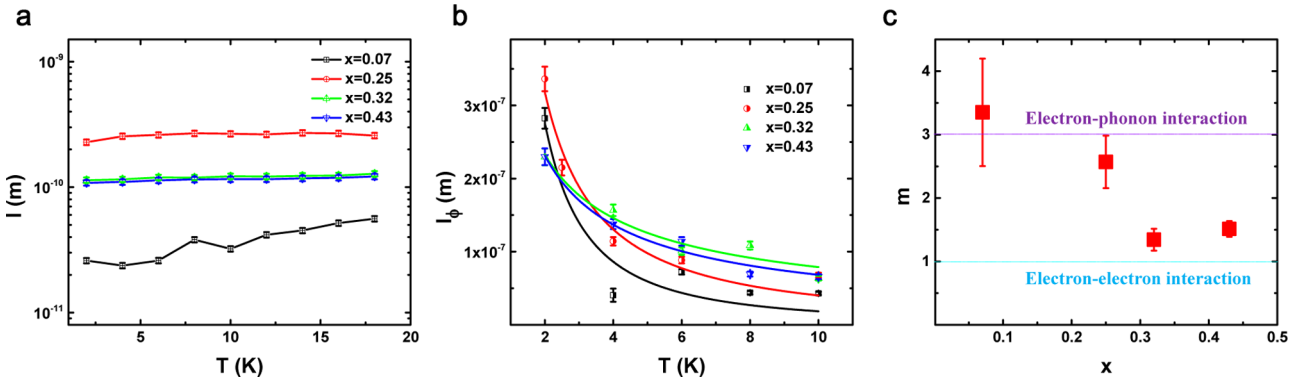

Figure 4. Transport parameters of the 16 nm $Pb_{1-x}Sn_xSe$ thin films. (a) Mean free path of 16 nm $Pb_{1-x}Sn_xSe$ thin films at different temperatures. (b) Phase coherence length of 16 nm $Pb_{1-x}Sn_xSe$ thin films at different temperatures. Solid curves are the fittings to the solid symbols with $l_\phi \propto T^{-m/2}$. (c) The fitted exponent m of different compositions.

phase will become $\phi = \pi[1 - (\Delta/(2E_F))]$, where Δ is the gap size and E_F is Fermi energy or the energy difference between Fermi level and the gap center.[24,26] In accordance with the theory, we performed the magnetotransport measurements of two groups of samples with variations in thickness and composition to probe the conductivity contribution from the quantum interference (σ^{qi}). Figure 2b shows the normalized MC $\sigma(B) - \sigma(0)$ of 10 nm $Pb_{1-x}Sn_xSe$ thin films with x = 0.07, 0.25, 0.32, and 0.43 at 2 K, while Figure 2c is that of 16 nm $Pb_{1-x}Sn_xSe$ thin films. According to the recent ARPES results,[2,5] x = 0.07 corresponds to the topological trivial states and x = 0.25, 0.32, and 0.43 possess the topological nontrivial states when in the bulk form. Figure 2b reveals a systematic crossover from WL to WAL at 2 K as x increases from 0.07 to 0.43 in 10 nm $Pb_{1-x}Sn_xSe$ thin films. Note that even though the resistance is beyond the quantum resistance range, we still use WL/WAL to describe the MC behavior because it is mainly originated from the quantum interference. The WL behavior in the 10 nm samples with x = 0.25 and 0.32 suggests that the top and bottom surfaces hybridize with each other giving rise to the surface gap (Δ) opening (Figure 2b). It has been predicted that as x increases, the penetration depth of the surface states decreases, resulting in a smaller surface gap.[17] Considering the insulating ground states in the 10 nm samples, the E_F is nearly independent of x and thus the Berry phase $\phi = \pi(1 - (\Delta/(2E_F)))$ is strongly subjected to the change of the surface gap Δ. Therefore, the Berry phase with the nontrivial value π tends to be present in highly doped and/or thicker samples with Δ close to zero (Figure 2b,c and Supporting Information Figure S3d,f,g). The entire trend from our MC curves (Figure 2b,c) agrees well with the projected change of Berry phase. Our results also verify a recent theoretical prediction that the TCI has a strong finite-size effect as compared to three-dimensional TIs such as Bi_2Se_3.[9] The size-sensitive nature of TCI states originates from the fact that the protection mechanism of surface states change from time reversal symmetry (in TIs) to crystal symmetry (in TCIs).

To further confirm the origin of the WL-WAL crossover, we use a back gate to tune the Fermi level and measure the MC under different gate voltages at 4 K (Figure 3a). All the samples exhibit a p-type conductivity. By applying a negative gate bias, the Fermi level moves toward valence band and $|E_F|$ becomes larger. Then the Berry phase ϕ acquires a value from the trivial state toward the nontrivial state continuously. Correspondingly, the MC changes from WL to WAL as shown in Figure 3a (dark yellow to black curves). Now, we can draw a conclusion that the complex magnetotransport behavior can be tuned by the Sn doping concentration, temperature, thickness, and gate voltage. All of them can affect the Berry phase and lead to a significant change in the low-field MC. Such a highly tunable Berry phase has never been realized in TI and can be used as a sensitive probe to study the electron transport behavior.[27,28]

Interestingly, MC experiences a clear transition of WAL weakening and WL emerging at the surface gapped samples as

DOI: 10.1021/acs.nanolett.5b00172
Nano Lett. XXXX, XXX, XXX−XXX

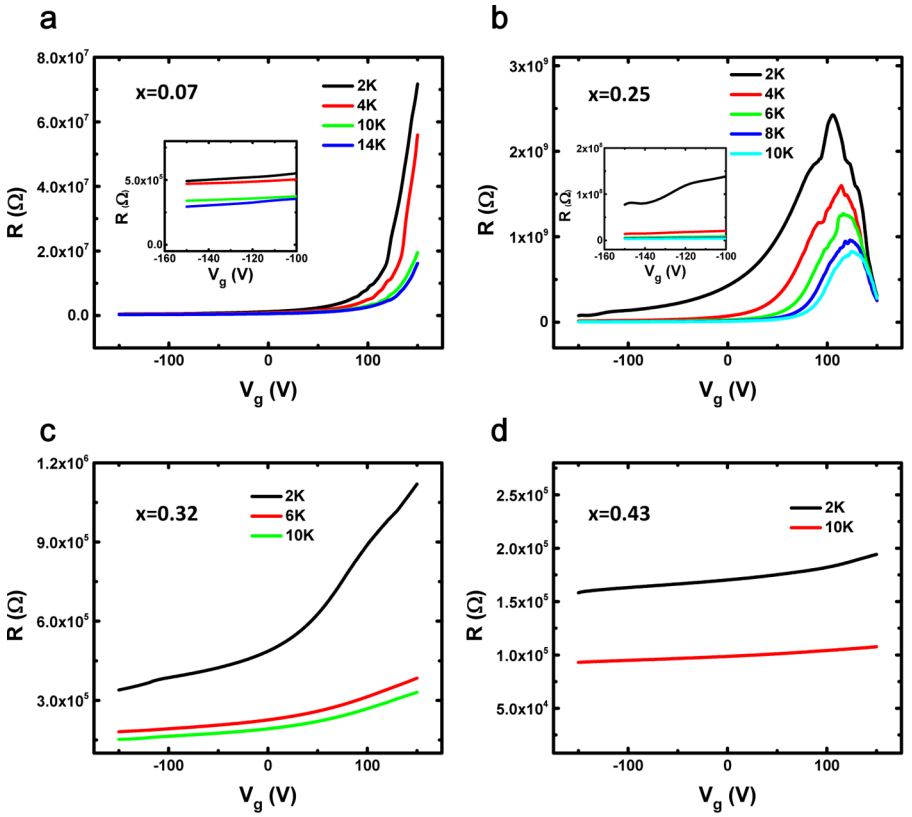

Figure 5. Channel resistance R versus gate voltage V_g at different temperatures in the 10 nm $Pb_{1-x}Sn_xSe$ thin films. (a–d) $R-V_g$ curve of 10 nm $Pb_{1-x}Sn_xSe$ thin films with x = 0.07, 0.25, 0.32, and 0.43, respectively. Insets show the enlarged off states of the $Pb_{1-x}Sn_xSe$ FET.

temperature decreases (Figure 3b and Supporting Information Figure S3a,c,e). At the first sight, one may consider that the Fermi level shifts relative to the valence band as the temperature is lowered. But according to the temperature-dependent carrier density (refer to Supporting Information Figure S4a), the Fermi energy stays almost the same in the temperature range of 2–20 K. Therefore, the Berry phase should not change much in T = 2–20 K. In the 2D system, the conductivity correction induced by quantum interference can be written as $|\sigma^{qi}| \propto (e^2/\pi h)\ln(l_\phi/l)$, where l_ϕ is phase coherence length and l is mean free path. l is determined by elastic scattering and it is not significantly affected by temperature.[29] From the Hall effect measurements, we can estimate l by the equation $l = (\hbar\mu/e)(3\pi^2 p_{2d}/d)^{1/3}$,[30] where d is the thickness of the thin film, e is the electron charge, and $\hbar$ is the reduced Planck's constant ($\hbar = h/2\pi$). From Figure 4a, one can find that the electron mean free path l in 16 nm $Pb_{1-x}Sn_xSe$ thin films is nearly independent of temperature. Nevertheless, l_φ is determined by the inelastic scattering that is influenced by temperature.[31] So the value of $|\sigma^{qi}|$ turns to be larger when the temperature decreases, which is consistent with Supporting Information Figure S3d,f,g,h, where the WAL(WL) behavior is notable at lower temperatures without any signs of transition. But the term σ^{qi} alone should not drive MC to the WAL/WL crossover. The previously neglected term σ^{ee} must be taken into consideration since the electron–electron interaction in $Pb_{1-x}Sn_xSe$ system is much stronger than the Bi-based TIs.[5] It is known that the MC correction σ^{ee} given by electron–electron interaction is always negative and proportional to the screening factor F, leading to WAL.[24] Thus, the WAL/WL crossover in Figure 3b can be explained as an interplay between σ^{ee} and σ^{qi} as follows: The term σ^{qi} plays a dominant role in MC, resulting in low temperature (2 K) WL behavior (Figure 3b) due to the trivial Berry phase, as discussed before. With the increase of temperature, the l_φ decreases logarithmically, resulting in the vanishing of σ^{qi}. And σ^{ee} becomes dominant in the conduction correction, which gives rise to WAL. Note that the bulk quantization contribution from the thin films can lead to WL in previous TIs.[32,33] So the bulk quantization may also contribute to the low-temperature WL.

The MR feature in most of our samples vanishes rapidly with temperature. At T = 30 K, the magnetic field fails to tune the resistance in most of our samples (not shown here). To study the dephasing mechanism in $Pb_{1-x}Sn_xSe$ system, we use an empirical formula $l_\phi \propto T^{-m/2}$ to fit l_ϕ, where m is positive and dependent on dephasing mechanism and dimensionality. If the dominant dephasing mechanism is the electron–electron interactions, then m = 1, or the electron–phonon interactions, then m = 3.[34] To avoid the fitting deviations of l_φ in the large resistance samples, we specially use the MC data of 16 nm $Pb_{1-x}Sn_xSe$ thin films for calculation (refer to Supporting Information Figure S4). By fitting the temperature-dependent l_ϕ (Figure 4b), m is found to be around 1.3–3.3 as shown in Figure 4c, which suggests the joint contributions of electron–electron and electron–phonon interactions. Moreover, increasing Sn doping concentration leads to the enhanced electron–electron interactions, as evidenced from the reduced value of m (closer to 1, Figure 4c). It is of interest to note that regardless of the dramatic variation of l (Figure 4a), l_ϕ has a negligible change with the doping concentration (Figure 4b) but stays several orders of magnitude higher than l. This points out that the elastic scattering dominates the transport property at low temperatures and the electrons preserve coherent phase after thousands of collisions even in the presence of strong disorder.

DOI: 10.1021/acs.nanolett.5b00172
Nano Lett. XXXX, XXX, XXX–XXX

Our results here also explain the observation of strong quantum oscillations in TCI nanowires with a large resistance well over the quantum resistance range.[35]

Besides the striking tunability of Berry phase, we also investigate the electric field effect on the resistance of the $Pb_{1-x}Sn_xSe$ thin films. Figure 5a-d show a typical R versus V_g curves of 10 nm $Pb_{1-x}Sn_xSe$ thin films at different temperatures. The on−off ratio increases as x becomes smaller. Importantly, we observe an ambipolar effect in 10 nm $Pb_{0.75}Sn_{0.25}Se$ thin films with a relatively high on−off ratio of 100 (taking the narrow band gap of the mother material into consideration). $Pb_{0.75}Sn_{0.25}Se$ is *p*-type at zero gate voltage. At 2 K, the R-V_g displays a turning point as the gate voltage is increased to 100 V. The decrease of R with increasing the gate voltage indicates the reverse of carrier type to electrons. The on−off ratio for both hole and electron conduction is more than 2 orders of magnitude, implying that the electronic states of the channel can be well modulated by electric field. The decreasing of the R-V_g curve is much faster than the increasing part. The asymmetric behavior for the hole and electron accumulation might result from the asymmetry in the density of states of valence band and conduction band.[1,2] The Fermi level, corresponding to the turning point, shifts toward valence band as temperature increases. This field effect transistor (FET) based on TCI shows a good tunability compared with previous TIs.[27,36,37] Our study is the first demonstration of TCI based FET and we observe a clear ambipolar gating effect with nearly perfect insulating off state. Further improvement of the FET performance can be done by reducing the channel size to nanoscale in combination with a top gate.

In conclusion, we have systematically investigated the doping and thickness induced topological phase transitions by electrical transport. We find a strong electron−electron interaction in the $Pb_{1-x}Sn_xSe$ system. Surface hybridization introduces a gap in the surface Dirac cone. We further clarify the origin of the Berry phase for the complicated MC transition between WAL and WL. Our results demonstrate a highly tunable Berry phase in $Pb_{1-x}Sn_xSe$ and pave the way for further exploring and manipulating this novel 2D TCI phase.

Methods. $Pb_{1-x}Sn_xSe$ thin films were epitaxially grown on dielectric $SrTiO_3$ (111) substrates in a PerkinElmer 425 molecular beam epitaxy (MBE) system with a base pressure of ca. 1×10^{-9} Torr. Pb, Sn, and Se fluxes were provided from standard Knudsen cells. The Pb/Sn ratio was determined by controlling cell temperatures of Pb and Sn. $SrTiO_3$ substrates were annealed at 400 °C for 30 min and kept at 250 °C during the growth. The growth rate was in situ monitored by the RHEED oscillations and ex situ checked by X-ray reflectivity measurement. The doping concentrations were determined by energy dispersive X-ray spectroscopy. The X-ray diffraction was obtained using Cu K_α radiation with Bruck D8 Discover X-ray diffraction system. Electrical transport measurements were performed in Physical Properties Measurement System (PPMS) with dc or low frequency (<200 Hz) ac lock-in technique.

■ ASSOCIATED CONTENT

Supporting Information

Figures of structure characterizations, fittings of low temperature resistance, normalized magnetoconductance, carrier density and HLN fitting parameters, and gate tunable magnetoconductance of $Pb_{1-x}Sn_xSe$ thin films. This material is available free of charge via the Internet at http://pubs.acs.org.

■ AUTHOR INFORMATION

Corresponding Author

*E-mail: faxian@fudan.edu.cn.

Notes

The authors declare no competing financial interest.

■ ACKNOWLEDGMENTS

This work was supported by the National Young 1000 Talent Plan, Pujiang Talent Plan in Shanghai, National Natural Science Foundation of China (61322407, 11474058), and the Chinese National Science Fund for Talent Training in Basic Science (J1103204). F.X. and C.Z. thank Liang Fu, Junwei Liu, Wenhui Duan, Jian Wang, and Shunqing Shen for helpful discussions. C.Z. appreciates Peihong Cheng, Zhigang Chen, Alexei V. Fedorov, Juan Jiang, and Yao Shen for helps in material characterizations.

■ REFERENCES

(1) Okada, Y.; Serbyn, M.; Lin, H.; Walkup, D.; Zhou, W.; Dhital, C.; Neupane, M.; Xu, S.; Wang, Y. J.; Sankar, R.; Chou, F.; Bansil, A.; Hasan, M. Z.; Wilson, S. D.; Fu, L.; Madhavan, V. *Science* **2013**, *341* (6153), 1496−9.

(2) Dziawa, P.; Kowalski, B. J.; Dybko, K.; Buczko, R.; Szczerbakow, A.; Szot, M.; Lusakowska, E.; Balasubramanian, T.; Wojek, B. M.; Berntsen, M. H.; Tjernberg, O.; Story, T. *Nat. Mater.* **2012**, *11* (12), 1023−7.

(3) Tanaka, Y.; Ren, Z.; Sato, T.; Nakayama, K.; Souma, S.; Takahashi, T.; Segawa, K.; Ando, Y. *Nat. Phys.* **2012**, *8* (11), 800−803.

(4) Wojek, B.; Dziawa, P.; Kowalski, B.; Szczerbakow, A.; Black-Schaffer, A.; Berntsen, M.; Balasubramanian, T.; Story, T.; Tjernberg, O. 2014, arXiv preprint arXiv:1401.6643 (accessed Sep 26, 2014).

(5) Neupane, M.; Xu, S.-Y.; Sankar, R.; Gibson, Q.; Wang, Y.; Alidoust, N.; Bian, G.; Liu, C.; Belopolski, I.; Ohtsubo, Y.; Taleb-Ibrahimi, A.; Basak, S.; Tsai, W.-F.; Lin, H.; Cava, R. J.; Bansil, A.; Chou, F. C.; Hasan, M. Z..; 2014, arXiv preprint arXiv:1403.1560 (accessed Sep 25, 2014).

(6) Xu, S. Y.; Liu, C.; Alidoust, N.; Neupane, M.; Qian, D.; Belopolski, I.; Denlinger, J. D.; Wang, Y. J.; Lin, H.; Wray, L. A.; Landolt, G.; Slomski, B.; Dil, J. H.; Marcinkova, A.; Morosan, E.; Gibson, Q.; Sankar, R.; Chou, F. C.; Cava, R. J.; Bansil, A.; Hasan, M. Z. *Nat. Commun.* **2012**, *3*, 1192.

(7) Yan, C.; Liu, J.; Zang, Y.; Wang, J.; Wang, Z.; Wang, P.; Zhang, Z.-D.; Wang, L.; Ma, X.; Ji, S. *Phys. Rev. Lett.* **2014**, *112* (18), 186801.

(8) Liu, J.; Hsieh, T. H.; Wei, P.; Duan, W.; Moodera, J.; Fu, L. *Nat. Mater.* **2014**, *13* (2), 178−83.

(9) Ozawa, H.; Yamakage, A.; Sato, M.; Tanaka, Y. *Phys. Rev. B* **2014**, *90* (4), 045309.

(10) Taskin, A. A.; Yang, F.; Sasaki, S.; Segawa, K.; Ando, Y. *Phys. Rev. B* **2014**, *89* (12), 121302.

(11) Assaf, B. A.; Katmis, F.; Wei, P.; Satpati, B.; Zhang, Z.; Bennett, S. P.; Harris, V. G.; Moodera, J. S.; Heiman, D. *Appl. Phys. Lett.* **2014**, *105*, 102108.

(12) Hasan, M. Z.; Kane, C. L. *Rev. Mod. Phys.* **2010**, *82* (4), 3045.

(13) Qi, X.-L.; Zhang, S.-C. *Rev. Mod. Phys.* **2011**, *83* (4), 1057.

(14) Fu, L. *Phys. Rev. Lett.* **2011**, *106* (10), 106802.

(15) Hsieh, T. H.; Lin, H.; Liu, J.; Duan, W.; Bansil, A.; Fu, L. *Nat. Commun.* **2012**, *3*, 982.

(16) Fang, C.; Gilbert, M. J.; Bernevig, B. A. *Phys. Rev. Lett.* **2014**, *112* (4), 046801.

(17) Serbyn, M.; Fu, L. *Phys. Rev. B* **2014**, *90* (3), 035402.

(18) Albers, W.; Haas, C.; Ober, H.; Schodder, G.; Wasscher, J. *J. Phys. Chem. Solids* **1962**, *23* (3), 215−220.

(19) Zhang, Y.; He, K.; Chang, C.-Z.; Song, C.-L.; Wang, L.-L.; Chen, X.; Jia, J.-F.; Fang, Z.; Dai, X.; Shan, W.-Y. *Nat. Phys.* **2010**, *6* (8), 584−588.

(20) Liu, C.-X.; Zhang, H.; Yan, B.; Qi, X.-L.; Frauenheim, T.; Dai, X.; Fang, Z.; Zhang, S.-C. *Phys. Rev. B* **2010**, *81* (4), 041307.

DOI: 10.1021/acs.nanolett.5b00172
Nano Lett. XXXX, XXX, XXX−XXX

(21) Sakudo, T.; Unoki, H. *Phys. Rev. Lett.* **1971**, *26* (14), 851−853.
(22) Liu, M.; Chang, C.-Z.; Zhang, Z.; Zhang, Y.; Ruan, W.; He, K.; Wang, L.-l.; Chen, X.; Jia, J.-F.; Zhang, S.-C.; Xue, Q.-K.; Ma, X.; Wang, Y. *Phys. Rev. B* **2011**, *83* (16), 165440.
(23) Wang, J.; DaSilva, A. M.; Chang, C.-Z.; He, K.; Jain, J. K.; Samarth, N.; Ma, X.-C.; Xue, Q.-K.; Chan, M. H. W. *Phys. Rev. B* **2011**, *83* (24), 245438.
(24) Lu, H.-Z.; Shen, S.-Q. *Phys. Rev. Lett.* **2014**, *112* (14), 146601.
(25) Ghaemi, P.; Mong, R. S.; Moore, J. E. *Phys. Rev. Lett.* **2010**, *105* (16), 166603.
(26) Lu, H.-Z.; Shi, J.; Shen, S.-Q. *Phys. Rev. Lett.* **2011**, *107* (7), 076801.
(27) Chen, J.; Qin, H. J.; Yang, F.; Liu, J.; Guan, T.; Qu, F. M.; Zhang, G. H.; Shi, J. R.; Xie, X. C.; Yang, C. L.; Wu, K. H.; Li, Y. Q.; Lu, L. *Phys. Rev. Lett.* **2010**, *105* (17), 176602.
(28) Steinberg, H.; Laloë, J. B.; Fatemi, V.; Moodera, J. S.; Jarillo-Herrero, P. *Phys. Rev. B* **2011**, *84* (23), 233101.
(29) Lu, H.-Z.; Shen, S.-Q. *Proc. SPIE* **2014**, 9167, Spintronics VII, 91672E.
(30) Brahlek, M.; Bansal, N.; Koirala, N.; Xu, S.-Y.; Neupane, M.; Liu, C.; Hasan, M. Z.; Oh, S. *Phys. Rev, Lett.* **2012**, *109* (18), 186403.
(31) Thouless, D. *Phys. Rev. Lett.* **1977**, *39* (18), 1167.
(32) Zhang, L.; Dolev, M.; Yang, Q. I.; Hammond, R. H.; Zhou, B.; Palevski, A.; Chen, Y.; Kapitulnik, A. *Phys. Rev. B* **2013**, *88* (12), 121103.
(33) Lu, H.-Z.; Shen, S.-Q. *Phys. Rev. B* **2011**, *84* (12), 125138.
(34) Lee, P. A.; Ramakrishnan, T. *Rev. Mod. Phys.* **1985**, *57* (2), 287.
(35) Safdar, M.; Wang, Q.; Mirza, M.; Wang, Z.; Xu, K.; He, J. *Nano Lett.* **2013**, *13* (11), 5344−9.
(36) Xiu, F.; He, L.; Wang, Y.; Cheng, L.; Chang, L. T.; Lang, M.; Huang, G.; Kou, X.; Zhou, Y.; Jiang, X.; Chen, Z.; Zou, J.; Shailos, A.; Wang, K. L. *Nat. Nanotechnol.* **2011**, *6* (4), 216−21.
(37) Wang, Y.; Xiu, F.; Cheng, L.; He, L.; Lang, M.; Tang, J.; Kou, X.; Yu, X.; Jiang, X.; Chen, Z.; Zou, J.; Wang, K. L. *Nano Lett.* **2012**, *12* (3), 1170−5.

DOI: 10.1021/acs.nanolett.5b00172
Nano Lett. XXXX, XXX, XXX−XXX